2.6 Gaussian Beams and Resonators

2.6.1 Gaussian Beam Propagation

The propagation of Gaussian beams through paraxial optical systems can be efficiently evaluated using the ABCD-law [4], which states that the q-parameter of a Gaussian beam passing a optical system described by an ABCD-marix is given by

$$q_2 = \frac{Aq_1 + B}{Cq_1 + D}, \tag{2.259}$$

where q_1 and q_2 are the beam parameters at the input and the output planes of the optical system or component, see Figure 2.72

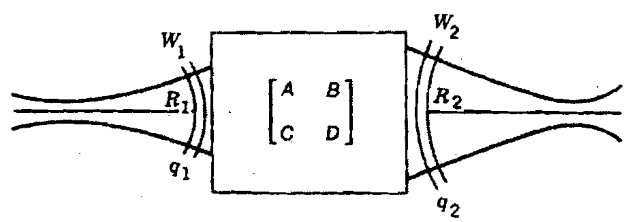

Figure 2.72: Gaussian beam transformation by ABCD law, [6], p. 99.

To proove this law, we realize that it is true for the case of free space propagation, i.e. pure diffraction, comparing (2.259) with (2.229) and (2.246). If we can proove that it is additionally true for a thin lens, then we are finished, because every ABCD matrix (2x2 matrix) can be written as a product of a lower and upper triangular matrix (LR-decomposition) like the one for free space propagation and the thin lens. Note, the action of the lens is identical to the action of free space propagation, but in the Fourier-domain. In the Fourier domain the Gaussian beam parameter is replaced by its inverse (2.222)

$$\widetilde{E}_0(x, y, z) = \frac{j}{q(z)} \exp\left[-jk_0\left(\frac{x^2 + y^2}{2q(z)}\right)\right]. \tag{2.260}$$

$$\widetilde{E}_0(k_z, k_y, z) = 2\pi j \exp\left[-jq(z)\left(\frac{k_z^2 + k_y^2}{2k_0}\right)\right] \tag{2.261}$$

But the inverse q-parameter transforms according to (2.259)

$$\frac{1}{q_2} = \frac{D\frac{1}{q_1} + C}{B\frac{1}{q_1} + A}, \tag{2.262}$$

which leads for a thin lens to

$$\frac{1}{q_2} = \frac{1}{q_1} - \frac{1}{f}. \tag{2.263}$$

This is exactly what a thin lens does, see Eq.(2.225), it changes the radius of curvature of the phase front but not the waist of the beam according to

$$\frac{1}{R_2} = \frac{1}{R_1} - \frac{1}{f}. \tag{2.264}$$

With that finding, we have proven the ABCD law for Gaussian beam propagation through paraxial optical systems.

The ABCD-matrices of the optical elements discussed so far including nonnomal incidence are summarized in Table 2.6. As an application of the

Optical Element	ABCD-Matrix
Propagation in Medium with index n and length L	$\begin{pmatrix} 1 & L/n \\ 0 & 1 \end{pmatrix}$
Thin Lens with focal length f	$\begin{pmatrix} 1 & 0 \\ -1/f & 1 \end{pmatrix}$
Mirror under Angle θ to Axis and Radius R Sagittal Plane	$\begin{pmatrix} 1 & 0 \\ \frac{-2\cos\theta}{R} & 1 \end{pmatrix}$
Mirror under Angle θ to Axis and Radius R Tangential Plane	$\begin{pmatrix} 1 & 0 \\ \frac{-2}{R\cos\theta} & 1 \end{pmatrix}$
Brewster Plate under Angle θ to Axis and Thickness d, Sagittal Plane	$\begin{pmatrix} 1 & \frac{d}{n} \\ 0 & 1 \end{pmatrix}$
Brewster Plate under Angle θ to Axis and Thickness d, Tangential Plane	$\begin{pmatrix} 1 & \frac{d}{n^3} \\ 0 & 1 \end{pmatrix}$

Table 2.6: ABCD matrices for commonly used optical elements.

Gaussian beam propagation, lets consider the imaging of a Gaussian beam with a waist w_{01} by a thin lens at a distance d_1 away from the waist to a beam with a different size w_{02}, see Figure 2.73.

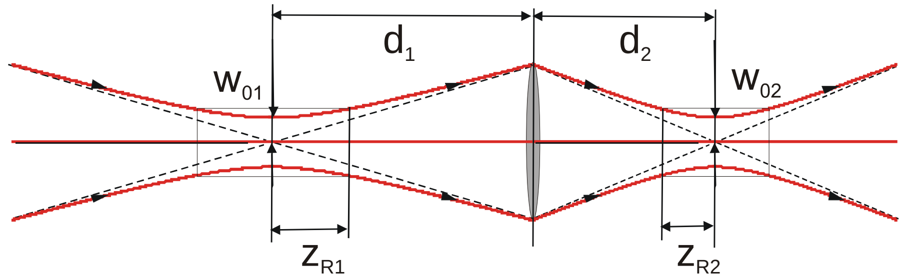

Figure 2.73: Focusing of a Gaussian beam by a lens.

There will be a new focus at a distance d_2.The corresponding ABCD matrix is of course the one from Eq.(2.257), which is repeated here

$$\begin{pmatrix} A & B \\ C & D \end{pmatrix} = \begin{pmatrix} 1 - \frac{d_2}{f} & \left(1 - \frac{d_2}{f}\right) d_1 + d_2 \\ -\frac{1}{f} & 1 - \frac{d_1}{f} \end{pmatrix}. \tag{2.265}$$

The q-parameter of the Gaussian beam at the position of minimum waist is purely imaginary $q_1 = jz_{R1} = j\frac{\pi w_{01}^2}{\lambda}$ and $q_2 = jz_{R2} = j\frac{\pi w_{02}^2}{\lambda}$, where

$$q_2 = \frac{A\ q_1 + B}{C\ q_1 + D} = \frac{jz_{R1}A + B}{jz_{R1}C + D} = \frac{jz_{R1}A + B}{jz_{R1}C + D} = jz_{R2}. \tag{2.266}$$

In the limit of ray optics, where the beam waists can be considered to by zero, i.e. $z_{R1} = z_{R2} = 0$ we obtain $B = 0$, i.e. the imaging rule of classical ray optics Eq.(2.256). It should not come at a surprise that for the Gaussian beam propagation this law does not determine the exact distance d_2 of the position of the new waist. Because, in the ray analysis we neglected diffraction. Therefore, the Gaussian beam analysis, although it uses the same description of the optical components, gives a slightly different and improved answer for the position of the focal point. To find the position d_2, we request that the real part of the right hand side of (2.266) is zero,

$$BD - z_{R1}^2 AC = 0 \tag{2.267}$$

which can be rewritten as

$$\frac{1}{d_2} = \frac{1}{f} - \frac{1}{d_1 + \frac{z_{R1}^2}{d_1 - f}}. \tag{2.268}$$

Again for $z_{R1} \to 0$, we obtain the ray optics result. And the imaginary part of Eq.(2.266) leads to

$$\frac{1}{z_{R2}} = \frac{1}{z_{R1}} \left(D^2 + z_{R1}^2 C^2 \right), \tag{2.269}$$

or

$$\frac{1}{w_{02}^2} = \frac{1}{w_{01}^2} \left(1 - \frac{d_1}{f} \right)^2 \left[1 + \left(\frac{z_{R1}}{d_1 - f} \right)^2 \right]. \tag{2.270}$$

With the magnification M for the spot size, with is closely related to the Magnification M_r of ray optics, we can rewrite the results as

Magnification	$M = M_r/\sqrt{1+\xi^2}$, with $\xi = \frac{z_{R1}}{d_1 - f}$ and $M_r = \left\vert \frac{f}{d_1-f} \right\vert$
Beam waist	$w_{02} = M \cdot w_{01}$
Confocal parameter	$2z_{R2} = M^2\, 2z_{R2}$
Distance to focus	$d_2 - f = M^2\,(d_1 - f)$
Divergence	$\theta_{02} = \theta_{01}/M$

(2.271)

2.6.2 Resonators

With the Gaussian beam solutions, we can finally construct optical resonators with finite transverse extent, i.e. real Fabry-Perots, by inserting into the Gaussian beam, see Figure 2.74, curved mirrors with the proper radius of curvature, such that the beam is imaged upon itself.

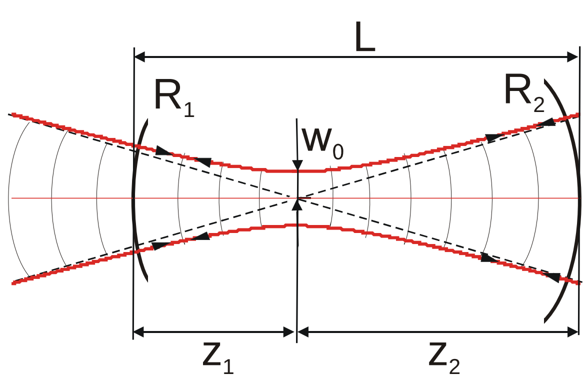

Figure 2.74: Fabry-Perot resonator with finite beam cross section by inserting curved mirrors into the beam to back reflect the beam onto itself.

Any resonator can be unfolded into a sequence of lenses and free space propagation. Here, we replace the curved mirrors by equivalent lenses with $f_1 = R_1/2$, and $f_2 = R_2/2$, see Figure 2.75.

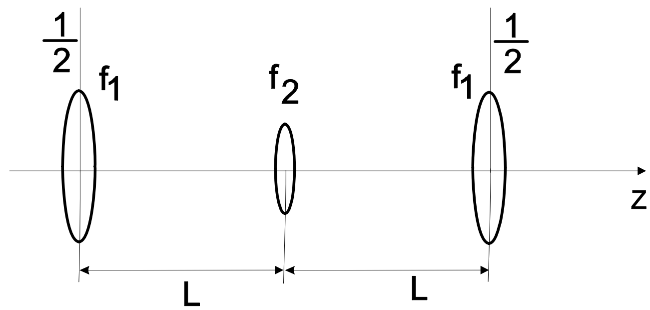

Figure 2.75: Two-mirror resonator unfolded. Note, only one half of the focusing strength of mirror 1 belongs to a fundamental period describing one resonator roundtrip.

The product of ABCD matrices describing one roundtrip of the beam in the resonator according to Figure 2.75 is

$$M = \begin{pmatrix} 1 & 0 \\ \frac{-1}{2f_1} & 1 \end{pmatrix} \begin{pmatrix} 1 & L \\ 0 & 1 \end{pmatrix} \begin{pmatrix} 1 & 0 \\ \frac{-1}{f_2} & 1 \end{pmatrix} \begin{pmatrix} 1 & L \\ 0 & 1 \end{pmatrix} \begin{pmatrix} 1 & 0 \\ \frac{-1}{2f_1} & 1 \end{pmatrix}. \qquad (2.272)$$

To carry out this product and to formulate the cavity stability criteria, it is convenient to use the cavity parameters $g_i = 1 - L/R_i, i = 1, 2$. The resulting cavity roundtrip ABCD-matrix can be written in the form

$$M = \begin{pmatrix} (2g_1g_2 - 1) & 2g_2L \\ 2g_1\left(g_1g_2 - 1\right)/L & (2g_1g_2 - 1) \end{pmatrix} = \begin{pmatrix} A & B \\ C & D \end{pmatrix}. \qquad (2.273)$$

Resonator Stability

The ABCD matrices describe the dynamics of rays propagating inside the resonator. The resonator is stable if no ray escapes after many round-trips, which is the case when the magnitude of the eigenvalues of the matrix M are less than one. Since we have a lossless resonator, i.e. $\det|M| = 1$, the product of the eigenvalues has to be 1 and, therefore, the stable resonator corresponds to the case of a complex conjugate pair of eigenvalues with a magnitude of 1. The eigenvalue equation to M is given by

$$\det|M-\lambda\cdot 1| = \det\left|\begin{pmatrix} (2g_1g_2-1)-\lambda & 2g_2L \\ 2g_1(g_1g_2-1)/L & (2g_1g_2-1)-\lambda \end{pmatrix}\right| = 0, \quad (2.274)$$

$$\lambda^2 - 2(2g_1g_2-1)\lambda + 1 = 0. \quad (2.275)$$

The eigenvalues are

$$\begin{aligned} \lambda_{1/2} &= (2g_1g_2-1) \pm \sqrt{(2g_1g_2-1)^2-1}, & (2.276) \\ &= \begin{cases} \exp(\pm\theta), \cosh\theta = 2g_1g_2-1, \text{ for } |2g_1g_2-1|>1 \\ \exp(\pm j\psi), \cos\psi = 2g_1g_2-1, \text{ for } |2g_1g_2-1|\le 1 \end{cases} & (2.277) \end{aligned}$$

The case of a complex conjugate pair corresponds to a stable resontor. Therefore, the stability criterion for a stable two mirror resonator is

$$|2g_1g_2-1| \le 1. \quad (2.278)$$

The stable and unstable parameter ranges are given by

$$\begin{aligned} \text{stable} &: \; 0 \le g_1\cdot g_2 = S \le 1 & (2.279) \\ \text{unstable} &: \; g_1g_2 \le 0; \text{ or } g_1g_2 \ge 1. & (2.280) \end{aligned}$$

where $S = g_1 \cdot g_2$, is the stability parameter of the cavity. The stability criterion can be easily interpreted geometrically. Of importance are the distances between the mirror mid-points M_i and the cavity end points, i.e. $g_i = (R_i - L)/R_i = -S_i/R_i$, as shown in Figure 2.76.

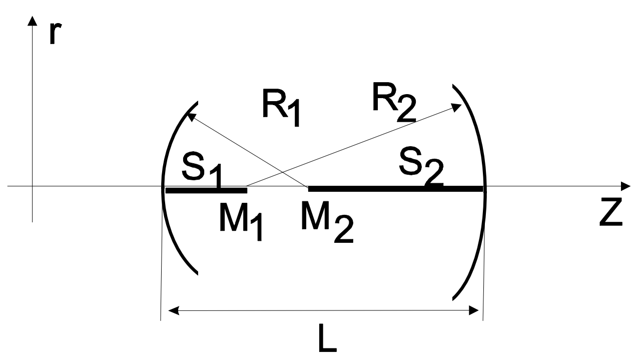

Figure 2.76: The stability criterion involves distances between the mirror mid-points M_i and the cavity end points. i.e. $g_i = (R_i - L)/R_i = -S_i/R_i$.

The following rules for a stable resonator can be derived from Figure 2.76 using the stability criterion expressed in terms of the distances S_i. Note, that the distances and radii can be positive and negative

$$\text{stable} : 0 \leq \frac{S_1 S_2}{R_1 R_2} \leq 1. \tag{2.281}$$

The rules are:

- A resonator is stable if the mirror radii, laid out along the optical axis, overlap.
- A resonator is unstable if the radii do not overlap or one lies within the other.

Figure 2.77 shows stable and unstable resonator configurations.

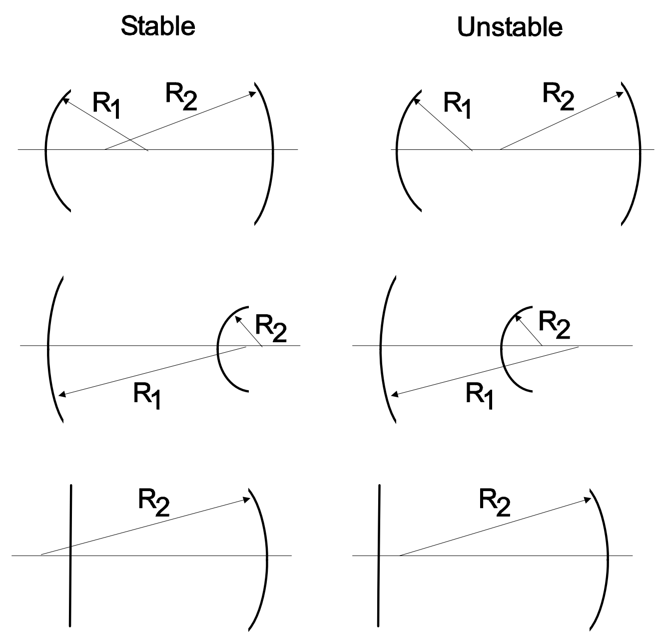

Figure 2.77: Illustration of stable and unstable resonator configurations.

For a two-mirror resonator with concave mirrors and $R_1 \leq R_2$, we obtain the general stability diagram as shown in Figure 2.78.

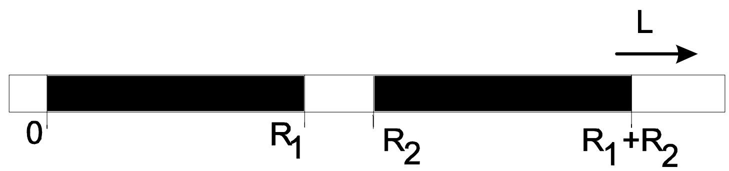

Figure 2.78: Stabile regions (black) for the two-mirror resonator.

There are two ranges for the mirror distance L, within which the cavity is stable, $0 \leq L \leq R_1$ and $R_2 \leq L \leq R_1 + R_2$. It is interesting to investigate the spot size at the mirrors and the minimum spot size in the cavity as a function of the mirror distance L.

Resonator Mode Characteristics

The stable modes of the resonator reproduce themselves after one round-trip, i.e.

$$q_1 = \frac{Aq_1 + B}{Cq_1 + D} \tag{2.282}$$

The inverse q-parameter, which is directly related to the phase front curvature and the spot size of the beam, is determined by

$$\left(\frac{1}{q}\right)^2 + \frac{A-D}{B}\left(\frac{1}{q}\right) + \frac{1-AD}{B^2} = 0. \tag{2.283}$$

The solution is

$$\left(\frac{1}{q}\right)_{1/2} = -\frac{A-D}{2B} \pm \frac{j}{2\,|B|}\sqrt{(A+D)^2 - 1} \tag{2.284}$$

If we apply this formula to (2.273), we find the spot size on mirror 1

$$\left(\frac{1}{q}\right)_{1/2} = -\frac{j}{2\,|B|}\sqrt{(A+D)^2 - 1} = -j\frac{\lambda}{\pi w_1^2}. \tag{2.285}$$

or

$$w_1^4 = \left(\frac{2\lambda L}{\pi}\right)^2 \frac{g_2}{g_1}\frac{1}{1-g_1 g_2} \tag{2.286}$$

$$= \left(\frac{\lambda R_1}{\pi}\right)^2 \frac{R_2 - L}{R_1 - L}\left(\frac{L}{R_1 + R_2 - L}\right). \tag{2.287}$$

By symmetry, we find the spot size on mirror 3 by switching index 1 and 2:

$$w_2^4 = \left(\frac{2\lambda L}{\pi}\right)^2 \frac{g_1}{g_2} \frac{1}{1-g_1 g_2} \tag{2.288}$$

$$= \left(\frac{\lambda R_2}{\pi}\right)^2 \frac{R_1 - L}{R_2 - L} \left(\frac{L}{R_1 + R_2 - L}\right). \tag{2.289}$$

The intracavity focus can be found by transforming the focused Gaussian beam with the propagation matrix

$$M = \begin{pmatrix} 1 & z_1 \\ 0 & 1 \end{pmatrix} \begin{pmatrix} 1 & 0 \\ \frac{-1}{2f_1} & 1 \end{pmatrix}$$

$$= \begin{pmatrix} 1 - \frac{z_1}{2f_1} & z_1 \\ \frac{-1}{2f_1} & 1 \end{pmatrix}, \tag{2.290}$$

to its new focus by properly choosing z_1, see Figure 2.74. A short calculation results in

$$z_1 = L \frac{g_2 (g_1 - 1)}{2g_1 g_2 - g_1 - g_2} \tag{2.291}$$

$$= \frac{L(L - R_2)}{2L - R_1 - R_2}, \tag{2.292}$$

and, again, by symmetry

$$z_2 = L \frac{g_1 (g_2 - 1)}{2g_1 g_2 - g_1 - g_2} \tag{2.293}$$

$$= \frac{L(L - R_1)}{2L - R_1 - R_2} = L - z_1. \tag{2.294}$$

The spot size in the intracavity focus is

$$w_o^4 = \left(\frac{\lambda L}{\pi}\right)^2 \frac{g_1 g_2 (1 - g_1 g_2)}{(2g_1 g_2 - g_1 - g_2)^2} \tag{2.295}$$

$$= \left(\frac{\lambda}{\pi}\right)^2 \frac{L(R_1 - L)(R_2 - L)(R_1 + R_2 - L)}{(R_1 + R_2 - 2L)^2}. \tag{2.296}$$

All these quantities for the two-mirror resonator are shown in Figure 2.79.

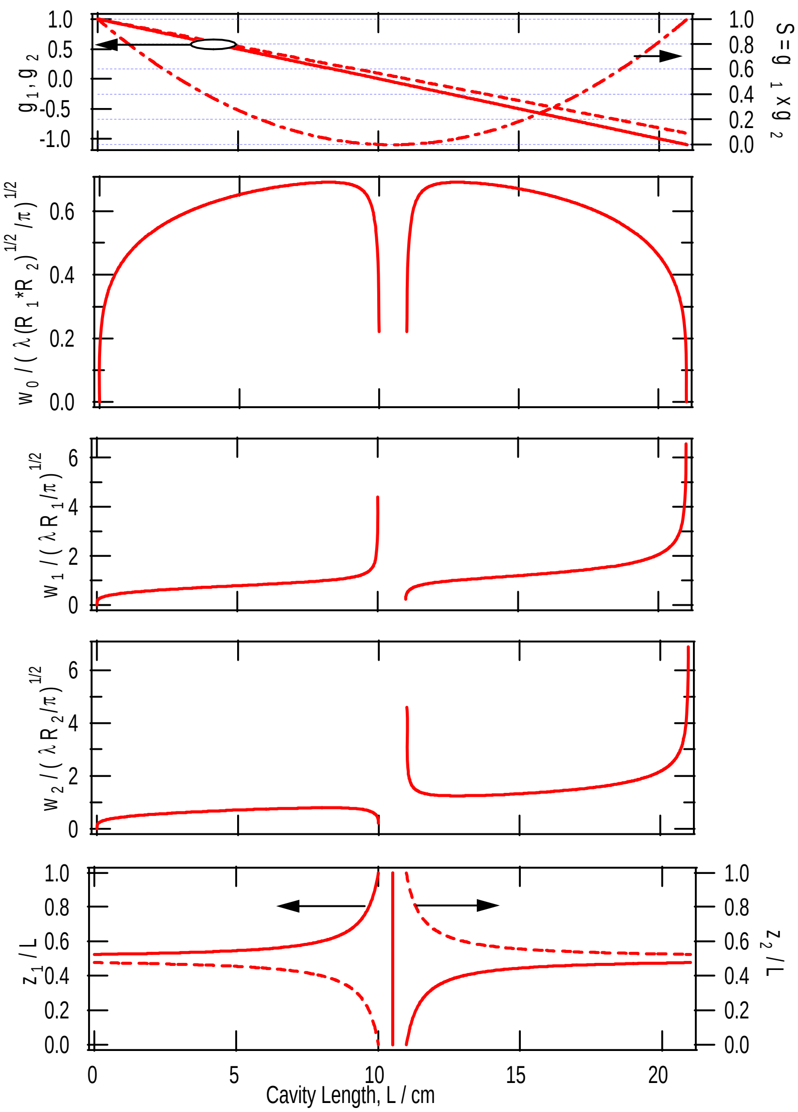

Figure 2.79: From top to bottom: Cavity parameters, g_1, g_2, S, w_0, w_1, w_2, z_1 and z_2 for the two-mirror resonator with $R_1 = 10$ cm and $R_2 = 11$ cm.

Hermite-Gaussian-Beams (TEM$_{pq}$-Beams)

It turns out that the Gaussian Beams are not the only solution to the paraxial wave equation (2.219). The stable modes of the resonator reproduce themselves after one round-trip,

$$\begin{aligned}\widetilde{E}_{l,m}(x,y,z) &= A_{l,m}\left[\frac{w_0}{w(z)}\right] G_l\left[\frac{\sqrt{2}x}{w(z)}\right] G_m\left[\frac{\sqrt{2}y}{w(z)}\right] \cdot \\ &\quad \exp\left[-jk_0\left(\frac{x^2+y^2}{2R(z)}\right)+j(l+m+1)\zeta(z)\right]\end{aligned} \quad (2.297)$$

where

$$G_l\left[u\right] = H_l\left[u\right]\exp\left[-\frac{u^2}{2}\right], \text{ for } l = 0,1,2,... \quad (2.298)$$

are the Hermite-Gaussians with the Hermite-Polynomials

$$\begin{aligned} H_0\left[u\right] &= 1, \\ H_1\left[u\right] &= 2u, \\ H_2\left[u\right] &= 4u^2-1, \\ H_3\left[u\right] &= 8u^3-12u, \end{aligned} \quad (2.299)$$

and $\zeta(z)$ is the Guoy-Phase-Shift according to Eq.(2.241). The lower order Hermite Gaussians are depicted in Figure 2.80

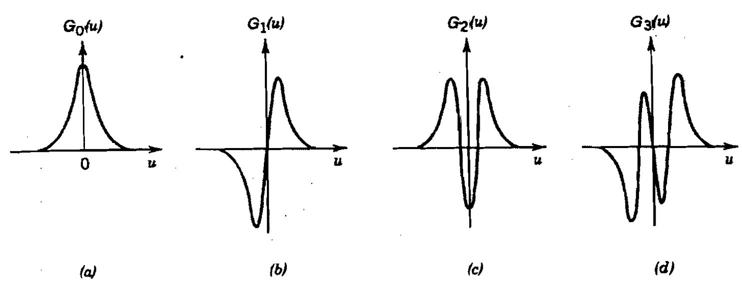

Figure 2.80: Hermite-Gauissians $G_l(u)$ for $l = 0, 1, 2$ and 3.

and the intensity profile of the first higher order resonator modes are shown in Figure 2.81.

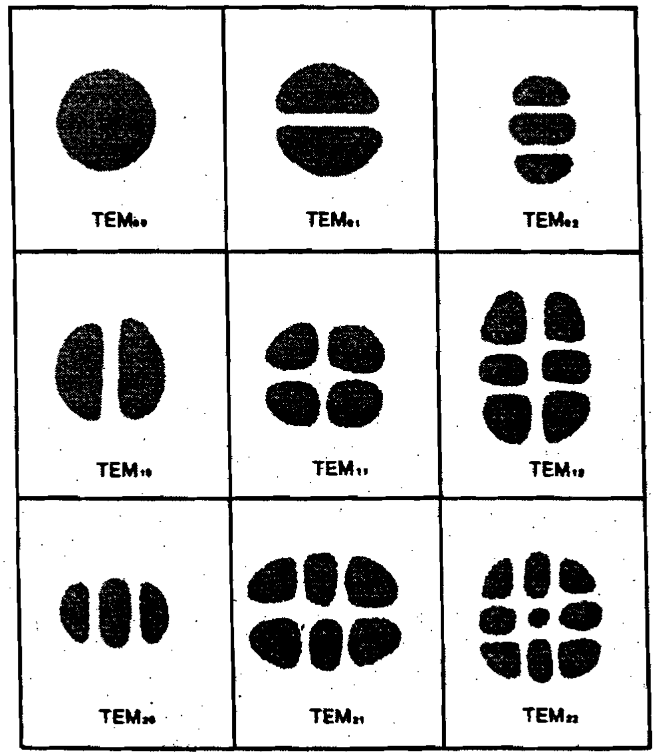

Figure 2.81: Intensity profile of TEM_{lm}-beams, [6], p. 103.

Besides the different mode profiles, the higher order modes experience greater phase advances during propogation, because they are made up of k-vectors with larger transverse components.

Axial Mode Structure

As we have seen for the Fabry-Perot resonator, the longitudinal modes are characterized by a roundtrip phase that is a multiple of 2π. Back then, we did not consider transverse modes. Thus in a resonator with finite transverse beam size, we obtain an extended family of resonances, with distinguishable field patterns. The resonance frequencies ω_{pmn} are determined by the roundtrip phase condition

$$\phi_{pmn} = 2p\pi, \text{ for } p = 0, \pm 1, \pm 2, ... \tag{2.300}$$

For the linear resonator according to Figure 2.74, the roundtrip phase of a Hermite-Gaussian T_{pmn}-beam is

$$\phi_{pmn} = 2kL - 2(m+n+1)\left(\zeta(z_2) - \zeta(z_1)\right), \tag{2.301}$$

where $\zeta(z_2) - \zeta(z_1)$ is the additional Guoy-Phase-Shift, when the beam goes through the focus once on its way from mirror 1 to mirror 2. Then the resonance frequences are

$$\omega_{pmn} = \frac{c}{L}\left[\pi p + (m+n+1)\left(\zeta(z_2) - \zeta(z_1)\right)\right]. \tag{2.302}$$

If the Guoy-Phase-Shift is not a rational number times π, then all resonance frequencies are non degenerate. However, for the special case where the two mirrors have identical radius of curvature R and are spaced a distance $L = R$ apart, which is called a confocal resonator, the Guoy-Phase-shift is $\zeta(z_2) - \zeta(z_1) = \pi/2$, with resonance frequencies

$$\omega_{pmn} = \frac{c}{L}\left[\pi p + (m+n+1)\frac{\pi}{2}\right]. \tag{2.303}$$

In that case all even, i.e. $m+n$, transverse modes are degenerate to the longitudinal or fundamental modes, see Figure 2.82.

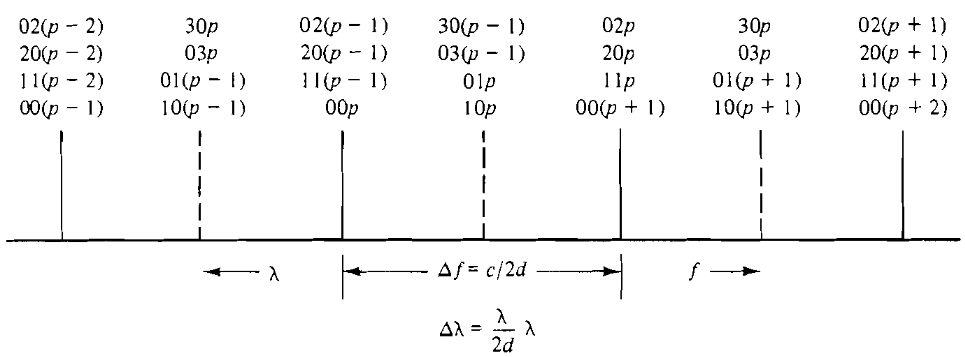

Figure 2.82: Resonance frequencies of the confocal Fabry-Perot resonator, [6], p. 128.

The odd modes are half way inbetween the longitudinal modes. Note, in contrast to the plan parallel Fabry Perot all mode frequencies are shifted by $\pi/2$ due to the Guoy-Phase-Shift.

2.7 Waveguides and Integrated Optics

As with electronics, miniaturization and integration of optics is desired to reduce cost while increasing functionality and reliability. One essential element is the guiding of the optical radiation in waveguides for integrated optical devices and optical fibers for long distance transmission. Waveguides can be as short as a few millimeters. Guiding of light with exceptionally low loss in fiber (0.1dB/km) can be achieved by using total internal reflection. Figure 2.83 shows different optical waveguides with a high index core material and low index cladding. The light will be guided in the high index core. Similar to the Gaussian beam the guided mode is made up of mostly paraxial plane waves that hit the high/low-index interface at grazing incidence and therefore undergo total internal reflections. The concomittant lensing effect overcomes the diffraction of the beam that would happen in free space and leads to stationary mode profiles fof the radiation.

Depending on the index profile and geometry one distinguishes between different waveguide types. Figure 2.83 (a) is a planar slab waveguide, which guides light only in one direction. This case is analyzed in more detail, as it has simple analytical solutions that show all phenomena associated with waveguiding such as cutoff, dispersion, single and multimode operation, coupling of modes and more, which are used later in devices and to achieve certain device properties. The other two cases show complete waveguiding in the transverse direction; (b) planar strip waveguide and (c) optical fiber.

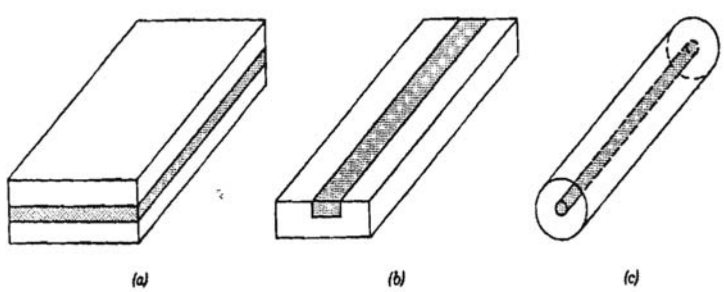

Figure 2.83: Dark shaded area constitute the high index regions. (a) planar slab waveguide; (b) strip waveguide; (c) optical fiber [6], p. 239.

In integrated optics many components are fabricated on a single sub-